

Phase transitions in a holographic superfluid model with non-linear terms beyond the probe limit

Zi-Qiang Zhao,^a Zhang-Yu Nie,^{b,1} Jing-Fei Zhang^{a,1} and Xin Zhang^{a,c,d,1}

^a*Key Laboratory of Cosmology and Astrophysics (Liaoning), College of Sciences, Northeastern University, Shenyang 110819, China*

^b*Center for Gravitation and Astrophysics, Kunming University of Science and Technology, Kunming 650500, China*

^c*Key Laboratory of Data Analytics and Optimization for Smart Industry (Ministry of Education), Northeastern University, Shenyang 110819, China*

^d*National Frontiers Science Center for Industrial Intelligence and Systems Optimization, Northeastern University, Shenyang 110819, China*

E-mail: zhaoziqiang@stumail.neu.edu.cn, niezy@kust.edu.cn,
jfzhang@mail.neu.edu.cn, zhangxin@mail.neu.edu.cn

ABSTRACT: We study the holographic s-wave superfluid model with 4th and 6th power self-interaction terms $\lambda|\psi|^4$ and $\tau|\psi|^6$ with considering the full back-reaction of the matter fields on the metric in the 3+1 dimensional bulk. The self-interaction terms are good at controlling the condensate to realize various phase transitions, such as the zeroth-order, first-order, and second-order phase transitions within the single condensate s-wave superfluid model. Therefore in this work, we are able to investigate the influence of the back-reaction strength on the various phase transitions, including the zeroth and first order phase transitions. In addition, we confirm that the influence of the 4th and 6th power terms on the superfluid phase transition in the case of finite back-reaction are qualitative the same as in the probe limit, thus present universality. We also plot the special value λ_s of the parameter λ at different back-reaction strength, below which the condensate grows to an opposite direction and is important in controlling the order of the superfluid phase transitions. Comparing the influence of the back-reaction parameter and that of the higher-order nonlinear coefficients, we see that the back-reaction strength brings in both the effective couplings similar to the 4th power and 6th power terms.

¹Corresponding authors.

Contents

1	Introduction	1
2	The holographic model	3
2.1	Equations of motion	3
2.2	Free energy	5
3	The power of the back-reaction strength on the various phase transitions	6
3.1	Second-order phase transition	6
3.2	Zeroth-order phase transitions and the power of τ	7
3.3	First-order phase transitions and the power of λ	8
3.4	COW phase transitions and the supercritical superfluid	9
4	The influence of λ and τ on phase transitions with finite back-reaction strength	11
5	Conclusions and discussions	13

1 Introduction

The AdS/CFT correspondence, introduced by J. M. Maldacena in 1997 [1], reveals an intrinsic connection between field theory and gravitational theory, which has provided a new perspective on understanding the nature of gravity and quantum matter. As a strong/weak duality, it is also regarded as a possible solution to strongly coupled problems. One of the most important applications of the AdS/CFT correspondence is the description of superconductor phase transitions, also known as the holographic superconductor model or the HHH model [2, 3]. The HHH model describes a simple s-wave superconductor that undergoes a second-order phase transition below the critical temperature T_c . Further studies have shown that in holographic systems, one can also realize p-wave [4, 5] and d-wave [6, 7] superconductors, as well as the coexistence and competition between multiple order parameters [8–15]. Additionally, different gravity backgrounds are explored in holographic superconductor models [16–20]. As a complete duality that helps us understand strongly coupled systems, the holographic models not only allow the study of equilibrium solutions but also provide insights into non-equilibrium dynamic evolution [21–25]. The AdS/CFT correspondence has also been used to study novel phenomena such as supersolid [26–30] and amorphous solid [31].

The other application of the AdS/CFT correspondence is to help better understand the nature of black hole and the underling laws of quantum gravity. As one of the most mysterious

yet simplest objects in the universe, the black holes have always been the most important project in the study of gravity. Despite extensive studies on black holes, some of the physical phenomena remain beyond the current theoretical framework, such as black hole singularities, black hole jets and black hole information paradox [32]. Additionally, black holes can serve as standard probes in cosmology to investigate our universe. For instance, gravitational waves produced by black hole mergers, often referred to as dark sirens [33–41]. It is absolutely important to study the dynamics of the metric fields in the study of the gravitational systems. Therefore, it is urgent and meaningful to extend the studies of holographic superfluids from the probe limit where the metric are fixed as the background to the complete case including the full back reaction of matter fields on the metric [3, 5, 17, 42–44]. The interplay between the matter and metric fields render the phase transition behavior of holographic superfluids more complex and more rich, such as introducing the reentrant phase transitions [14], first-order phase transitions [5, 14, 45, 46] and zeroth-order phase transitions [5, 46].

In a recent study on the holographic s-wave superfluid model [47], the authors use 4th and 6th power terms to achieve powerful control on the superfluid phase transitions in the probe limit, where usually only second-order phase transitions are realized. They explored the parameter space of this model where various phase transitions including second-order, first-order, zeroth-order phase transitions as well as “cave of wind” phase transitions appear. The linear stability of these phase transitions are also studied by calculating the quasi-normal modes, which confirm the landscape deduce from the free energy of the on-shell states. Later the full dynamical spinodal decomposition processes in this same model is realized in Ref. [24], which confirmed the inhomogeneous linear instability from the QNMs and the non-equilibrium creation and evolution of bubbles are observed. This same simple model is also utilized to study the problems in the supercritical region [48].

From the above progresses, it is interesting to study the simple s-wave superfluid model with 4th and 6th power terms with considering the back-reaction on metric. On one side, we are able to explore the control of the back-reaction strength on the various phase transitions, and on the other hand, we can test the universal control of the nonlinear terms on the phase transitions. Finally, it is also convenient to compare the influence of the back-reaction parameter and that of the nonlinear terms in such a setup, hence promote a better understanding on the effect of metric dynamics in the holographic phase transitions.

In this paper, we investigate the holographic superfluid model containing self-interaction terms with considering the full dynamics involving the metric and matter fields. The rest of this paper will be structured as follows. In Section 2, we present the holographic setup and the details of the calculations. In Section 3, we study the control of the back-reaction strength on the various phase transitions. In Section 4, we examine the universal control of the 4th and 6th power terms on the phase transitions at finite value of the back-reaction strength and give the dependence of the special value λ_s on the back-reaction strength. Finally, we provide some conclusions and discussions in Section 5.

2 The holographic model

2.1 Equations of motion

In Ref. [47], the second-order, first-order and zeroth-order phase transitions are easily realized with considering the 4th and 6th power scalar potential terms in the probe limit. In order to investigate the back-reaction of matter fields on the metric, we consider the following action including both the matter part S_M and the gravity part S_G

$$S = S_M + S_G, \quad S_G = \frac{1}{2\kappa_g^2} \int d^4x \sqrt{-g} (R - 2\Lambda), \quad (2.1)$$

$$S_M = \frac{1}{q^2} \int d^4x \sqrt{-g} \left(-\frac{1}{4} F_{\mu\nu} F^{\mu\nu} - D_\mu \psi^* D^\mu \psi - m^2 \psi^* \psi - \lambda (\psi^* \psi)^2 - \tau (\psi^* \psi)^3 \right). \quad (2.2)$$

Here, $F_{\mu\nu} = \nabla_\mu A_\nu - \nabla_\nu A_\mu$ is the Maxwell field strength and $D_\mu \psi = \nabla_\mu \psi - iA_\mu \psi$ is the standard covariant derivative term of the charged scalar ψ .

The Einstein equation is

$$R_{\mu\nu} - \frac{1}{2}(R - 2\Lambda)g_{\mu\nu} = b^2 \mathcal{T}_{\mu\nu}, \quad (2.3)$$

where $b = \kappa_g/q$ describes the strength of back-reaction of matter fields on the background geometry and $\kappa_g^2 = 8\pi G$. $\mathcal{T}_{\mu\nu}$ is the stress-energy tensor of the matter fields

$$\begin{aligned} \mathcal{T}_{\mu\nu} = & \left(-\frac{1}{4} F_{\alpha\beta} F^{\alpha\beta} - D_\alpha \psi^* D^\alpha \psi - m^2 \psi^* \psi - \lambda (\psi^* \psi)^2 - \tau (\psi^* \psi)^3 \right) g_{\mu\nu} \\ & + (D_\mu \psi^* D_\nu \psi + D_\nu \psi^* D_\mu \psi) + F_{\mu\alpha} F_\nu^\alpha. \end{aligned} \quad (2.4)$$

We use the standard ansatz for realizing the holographic superfluid phase transition

$$\psi = \psi(r), \quad A_\mu dx^\mu = \phi(r) dt, \quad (2.5)$$

and the line element is consistently set to

$$ds^2 = -N(r)\sigma(r)^2 dt^2 + \frac{1}{N(r)} dr^2 + r^2 dx^2 + r^2 dy^2, \quad (2.6)$$

with

$$N(r) = \frac{r^2}{L^2} \left(1 - \frac{2M(r)}{r^3} \right), \quad (2.7)$$

where L is the AdS radius. The Hawking temperature of such a black brane spacetime is

$$T = \frac{N'(r_h)\sigma(r_h)}{4\pi}, \quad (2.8)$$

where $r = r_h$ labels the position of the event horizon.

With the above ansatz, the full equations of motion can be written as

$$\begin{aligned} \psi''(r) = & \left(\frac{m^2}{N(r)} - \frac{\phi(r)^2}{N(r)^2 \sigma(r)^2} \right) \psi(r) + \frac{2\lambda}{N(r)} \psi(r)^3 + \frac{3\tau}{N(r)} \psi(r)^5 \\ & - \left(\frac{N'(r)}{N(r)} + \frac{2}{r} + \frac{\sigma'(r)}{\sigma(r)} \right) \psi'(r), \end{aligned} \quad (2.9)$$

$$\phi''(r) = \left(\frac{\sigma'(r)}{\sigma(r)} - \frac{2}{r} \right) \phi'(r) + \frac{2\psi(r)^2}{N(r)} \phi(r), \quad (2.10)$$

$$\sigma'(r) = b^2 r \left(\frac{\phi(r)^2 \psi(r)^2}{N(r)^2 \sigma(r)} + \sigma(r) \psi'(r)^2 \right), \quad (2.11)$$

$$\begin{aligned} M'(r) = & \frac{b^2 r^2}{\sigma(r)^2} \left(\frac{L^2 \phi(r)^2 \psi(r)^2}{2 N(r)} + \frac{L^2 \phi'(r)^2}{4} \right) + \frac{1}{2} b^2 r^2 L^2 (N(r) \psi'(r)^2 + m^2 \psi(r)^2) \\ & + \frac{1}{2} L^2 b^2 r^2 (\lambda \psi(r)^4 + \tau \psi(r)^6), \end{aligned} \quad (2.12)$$

with three sets of scaling symmetries:

$$\begin{aligned} (1) \quad & \phi \rightarrow a^2 \phi, \quad \psi \rightarrow a \psi, \quad N \rightarrow a^2 N, \quad m \rightarrow a m, \quad L \rightarrow a^{-1} L, \\ & b \rightarrow a^{-1} b, \quad \tau \rightarrow a^{-2} \tau. \\ (2) \quad & \phi \rightarrow a \phi, \quad \sigma \rightarrow a \sigma. \\ (3) \quad & \phi \rightarrow a \phi, \quad N \rightarrow a^2 N, \quad M \rightarrow a^3 M, \quad r \rightarrow a r. \end{aligned} \quad (2.13)$$

In order to solve these equations, we need to specify the boundary conditions on the horizon $r = r_h$ as well as on the asymptotic boundary $r \rightarrow \infty$. Without loss of generality, we set $L = 1$, $G = 1$ in the rest of this paper. We also set $r_h = 1$ in the numerical calculation and recover the value of r_h with the scaling symmetry (3) while the chemical potential μ or the charge density ρ are scaled to a fixed value. The expansion of the functions near the horizon are

$$\phi(r) = \phi_{h_1}(r - r_h) + \phi_{h_2}(r - r_h)^2 + \dots, \quad (2.14)$$

$$\psi(r) = \psi_{h_0} + \psi_{h_1}(r - r_h) + \dots, \quad (2.15)$$

$$\sigma(r) = \sigma_{h_0} + \sigma_{h_1}(r - r_h) + \dots, \quad (2.16)$$

$$M(r) = \frac{r_h^3}{2} + M_{h_1}(r - r_h) + \dots. \quad (2.17)$$

The horizon requires $N(r_h) = 0$, which is equal to $M(r_h) = \frac{r_h^3}{2}$. Near AdS boundary, the

expansion of functions are

$$\phi(r) = \mu - \frac{\rho}{r} + \dots, \quad (2.18)$$

$$\psi(r) = \frac{\psi^{(1)}}{r} + \frac{\psi^{(2)}}{r^2} + \dots, \quad (2.19)$$

$$\sigma(r) = \sigma_{b_0} + \frac{\sigma_{b_3}}{r^3} + \dots, \quad (2.20)$$

$$M(r) = M_{b_0} + \frac{M_{b_1}}{r} + \dots. \quad (2.21)$$

The scaling symmetry (2.13) will be used to rescale any solution to be asymptotically AdS, which means $\sigma(\infty) = 1$. The remaining boundary conditions are: $\psi(r_h) = -(3/2)\psi'(r_h) + M'(r_h)\psi'(r_h)$, $\psi^{(1)}(\infty) = 0$, $\phi(r_h) = 0$, $\phi(\infty) = \mu$, where μ is the chemical potential. With these boundary conditions, we can solve the equations of motion numerically.

In this paper, we choose the standard quantization scheme, which means $\psi^{(1)} = 0$ and the non-trivial vacuum expectation value is $\langle \mathcal{O} \rangle = \sqrt{2}\psi^{(2)}$.

2.2 Free energy

In this work, we choose to fix the value of the chemical potential μ and get solutions with various values of temperature T , which means we work in the grand canonical ensemble. An essential tool for confirming the order of a phase transition in the grand canonical ensemble is the grand potential. Therefore in this section, we provide the formula for calculating the grand potential density. The grand potential of this holographic system equals the temperature times the Euclidean on-shell action in the bulk spacetime [5, 14]

$$\Omega = TS_E, \quad (2.22)$$

where S_E is

$$S_E = \frac{1}{2\kappa_g^2} \int d^4x \sqrt{-g} (R - 2\Lambda + 2b^2 \mathcal{L}_{matter}) - \frac{1}{\kappa_g^2} \int d^3x \sqrt{-h} \left(K + \frac{2}{L} \right). \quad (2.23)$$

In Eq. (2.23), \mathcal{L}_{matter} is the Lagrange density of the matter part and K is the trace of the extrinsic curvature $K_{\mu\nu}$ for the boundary (see details in Refs. [14, 49]), where $K_{\mu\nu} = -h_\mu^\rho \nabla_\rho n_\nu$ and n is the unit normal to the boundary surface. By substituting the equations of motion into the action, one can derive the formula for the grand potential density at the boundary

$$\frac{2\kappa_g^2 \Omega}{V_2} = \lim_{r \rightarrow \infty} \left[2rN(r)\sigma(r) + r^2\sigma(r)N'(r) + 2r^2N(r)\sigma'(r) - 4r^2\sqrt{N(r)}\sigma(r) \right], \quad (2.24)$$

where V_2 is the area of the two dimensional transverse space. For the normal phase, the temperature and grand potential density are

$$T = \frac{r_h}{4\pi} \left(3 - \frac{b^2\mu^2}{2r_h^2} \right), \quad \frac{2\kappa_g^2 \Omega}{V_2} = -r_h^2 - \frac{1}{2}b^2\mu^2 r_h, \quad (2.25)$$

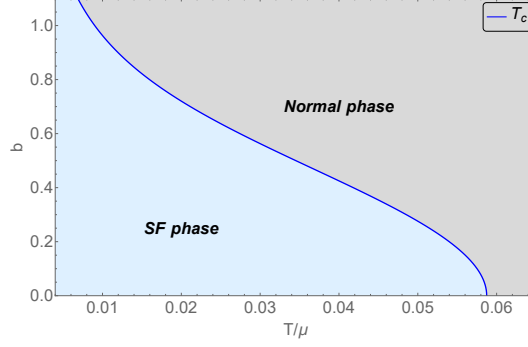


Figure 1: The phase diagram of temperature T/μ and back-reaction parameter b with $\lambda = 0$ and $\tau = 0$. The blue solid line represents the phase transition points of second-order phase transition.

while for the condensed phases, they are

$$T = \frac{r_h}{4\pi} \left(3\sigma_{h_0} - \frac{b^2 \phi_{h_1}^2}{2\sigma_{h_0}} - b^2 m^2 \sigma_{h_0} \psi_{h_0}^2 - b^2 \lambda \sigma_{h_0} \psi_{h_0}^4 - b^2 \tau \sigma_{h_0} \psi_{h_0}^6 \right),$$

$$\frac{2\kappa_g^2 \Omega}{V_2} = -2M_{b_0}. \quad (2.26)$$

When $b = 0$, the spacetime background will decouple from the matter fields, leading us back to the probe limit where the various phase transitions are realized in the previous study (see Ref. [47]).

3 The power of the back-reaction strength on the various phase transitions

3.1 Second-order phase transition

In this model, when the coefficients of the self-interaction terms λ and τ both equal to zero, only second-order phase transitions are realized. Since the back-reaction effect in this model has already been studied in Ref. [3], we only present the $b-T$ phase diagram in Figure 1, where we see that the relationship between critical temperature T_c and the back-reaction parameter b . It shows that the critical temperature T_c decrease with the increasing of the back-reaction parameter b . This feature tells us that the larger the back-reaction of matter fields on the background geometry, the more difficult it will be for the superfluid condensate to occur.

As the back-reaction increases, the critical temperature gradually approaches zero [3], simultaneously, the calculation of the condensate curve becomes more difficult. This numerical difficulty limits us to only considering a maximum value $b = 1.2$ for the back-reaction parameter. It is worth noting that the change in the back-reaction parameter not only affects the critical temperature but also alters the condensate curves.

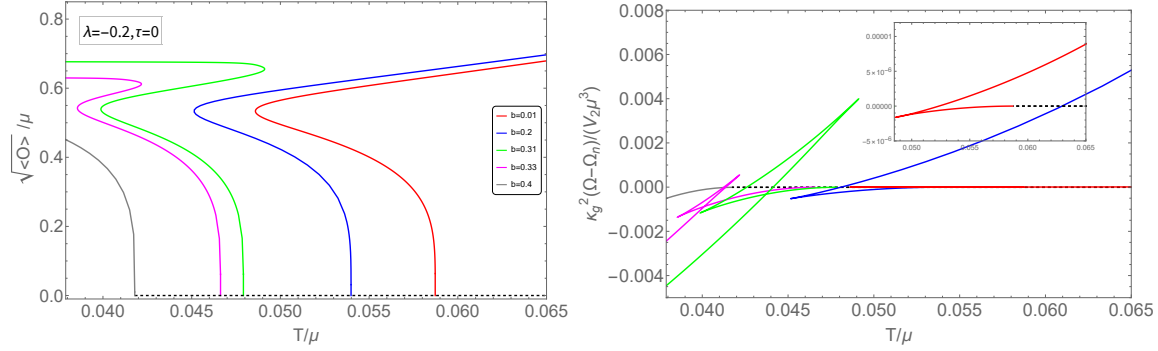


Figure 2: The dependence of the condensate curves on the back-reaction term b with parameters $\lambda = -0.2$ and $\tau = 0$. The left panel depicts the condensate diagram, while the right panel represents the corresponding free energy. The red, blue, green and magenta solid lines represent first-order phase transition. The gray solid lines represents second-order phase transition. The black dashed line is the normal solution.

3.2 Zeroth-order phase transitions and the power of τ

In the probe limit, with fixed parameters $\lambda = -0.2$ and $\tau = 0$, the system show a zeroth-order superfluid phase transition [47]. We further turn on the back-reaction with $\lambda = -0.2$ to see how the zeroth order phase transition changes with the increasing strength of the back-reaction. In Figure 2, we illustrate the the condensate curves with different values of the back-reaction parameter b for $\lambda = -0.2$ and $\tau = 0$. We see that as the back-reaction parameter b increases, the phase transition gradually changes from a zeroth-order phase transition to a first-order phase transition and finally becomes a second-order phase transition.

In Ref. [47], it has been discussed that when the self-interaction parameter λ is less than zero, it implies an intrinsic attractive interaction for large value of the order parameter ψ , leading the system to suffer the run away instability while undergoes a zeroth-order phase transition. This kind of instability in the zeroth-order phase transitions are confirmed from both the thermodynamic and dynamic perspectives [47]. One simple method to rescue the system from this run away instability is the introducing of an additional 6th power self-interaction term with a positive value of τ . This approach change the system from a zeroth-order phase transition to a first-order phase transition with a small value of τ or a second-order phase transition with a very large value of τ . Now we see the similar effect from the increasing value of back-reaction strength b .

The green and magenta curves clearly contain the character of a first-order phase transition and the gray curve show a typical second-order phase transition. Although the red and blue curves seem to be zeroth-order phase transitions, it is not confirmed that whether the curves will turn back at large condensate and become first-order phase transitions. Therefore we resort to the landscape analysis from the effective interaction of the back-reaction to confirm whether these phase transitions will turn to be first-order or not.

As discussed in Ref. [47], from the landscape perspective, it is clear that in the probe

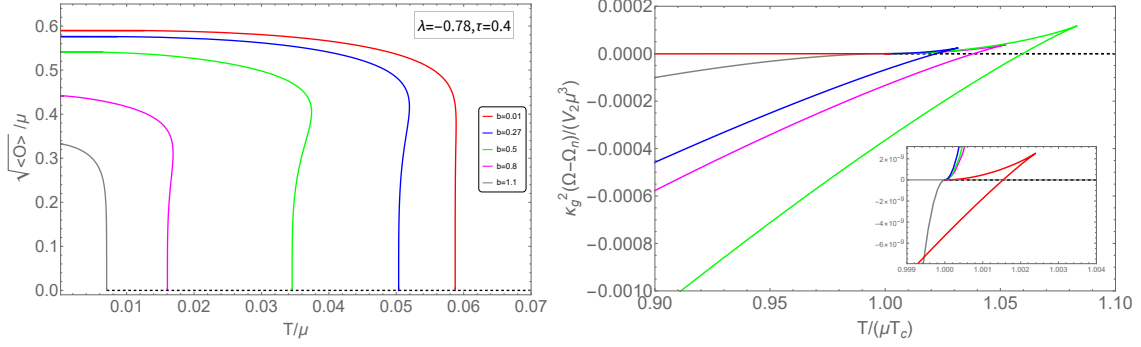


Figure 3: The dependence of the condensate curves on the back-reaction term b with parameters $\lambda = -0.78$ and $\tau = 0.4$. The left panel depicts the condensate diagram, while the right panel represents the corresponding free energy. The red, blue, green and magenta solid lines represent first-order phase transition. The gray solid line represents second-order phase transition. The black dashed line is the normal solution.

limit of the zero-order phase transition, as long as there is a positive τ , no matter how small it is, it will always stabilize the system by bounding the thermodynamic potential landscape from below. If the back-reaction on the metric bring in similar effective self-interaction, a condensate solution with very large value of $\langle \mathcal{O} \rangle$ always exist in the low temperature region, and the condensate curve will always turn back to form a style of the standard first-order phase transition. Due to numerical limitations, we cannot get solutions with arbitrarily large value of $\langle \mathcal{O} \rangle$ to demonstrate this directly, however, we are able to confirm such a similar effective self-interaction of the back-reaction from the green, magenta and gray curves in Figure 2. Therefore, we suppose that the phase transitions with finite back-reaction strength, such as the red and blue cases in Figure 2 indicate first-order phase transitions. Nevertheless, the back-reaction of the matter fields on the spacetime background exhibits more complex influences than the higher power nonlinear potential terms. When the back-reaction parameter is changed, the critical temperature T_c of the system also changes simultaneously. In contrary, higher-order nonlinear terms only influence the configuration of the condensate curves of the system without altering the critical temperature.

3.3 First-order phase transitions and the power of λ

In the above subsection, we confirmed that the back-reaction bring in effective interactions similar to the 6th (or higher) power potential term. To confirm whether the back-reaction also bring in effective interactions similar to the 4th power term, which is important in switching the superfluid phase transitions between the second-order and first-order phase transitions [47], we set the value λ to be close to the special value $\lambda_s = -0.757$ in the probe limit, which controls whether the condensate curve grows leftwards or rightwards at the critical point. Then we see whether the growing direction change with the back-reaction strength or not.

We first set $\lambda = -0.78$ and $\tau = 0.4$, where λ is slightly lower than the special value λ_s in

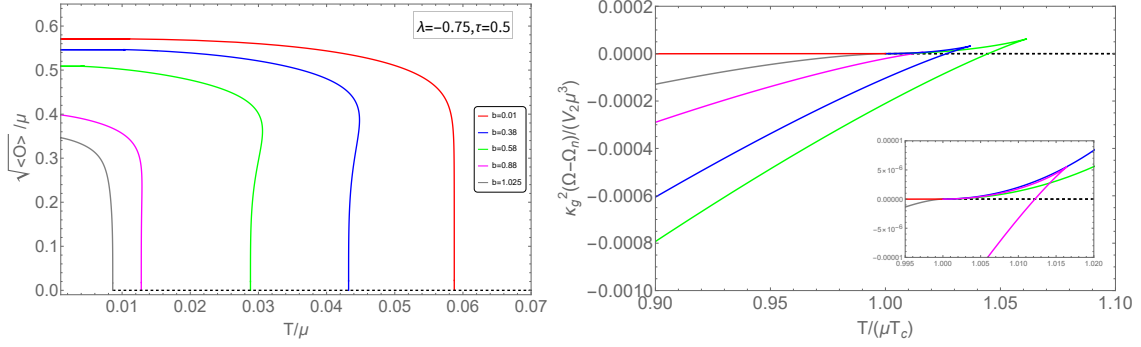


Figure 4: The dependence of the condensate curves on the back-reaction term b with parameters $\lambda = -0.75$ and $\tau = 0.5$. The left panel depicts the condensate diagram, while the right panel represents the corresponding free energy. The red and gray solid lines represent second-order phase transition. The blue, green and magenta solid lines represents first-order phase transition. The black dashed line is the normal solution.

the probe limit. In this case, the phase transition in the probe limit is first-order. We further present the condensates as well as the grand potential curves with increasing values of the back-reaction strength in Figure 3. It is clear that along with the increasing value of the back-reaction strength, the superfluid phase transition remains first-order with the decreasing of the quasi-critical point. To show the first-order phase transitions more clearly, we normalized the temperature with respect to T_c in the right panel for the grand potential curves.

In the next step, we set $\lambda = -0.75$ and $\tau = 0.5$, where λ is slightly higher than the special value λ_s . In this case, the phase transition in the probe limit is second-order instead. We present the condensates as well as the grand potential curves with increasing values of the back-reaction strength b in Figure 4. We see that along with the increasing value of the back-reaction strength b from the probe limit, the superfluid phase transition change from the second-order to first-order. Interestingly, with the back-reaction strength continuously growing to a large enough value, the superfluid phase transition turns back to be second-order. We further present a $b - T$ phase diagram in Figure 5 to show this interesting behavior more clearly. From this phase diagram we can see two red points at the end of the first-order phase transitions, which indicates a non-monotonic control on the condensate near the critical point from the back-reaction strength similar to the 4th power term with coefficient λ .

3.4 COW phase transitions and the supercritical superfluid

Following the above analysis of back-reaction effects on zeroth-order, first-order and second-order phase transitions, we continue our study on the final case: the COW phase transitions. With $0 > \lambda > \lambda_s$ and a small positive value of τ , the condensate curve show a COW configuration. At this time, the system undergoes a second-order superfluid phase transition from the normal phase, as well as a first-order phase transition between two superfluid phases with different values of condensate. It is confirmed that the first-order phase transition between

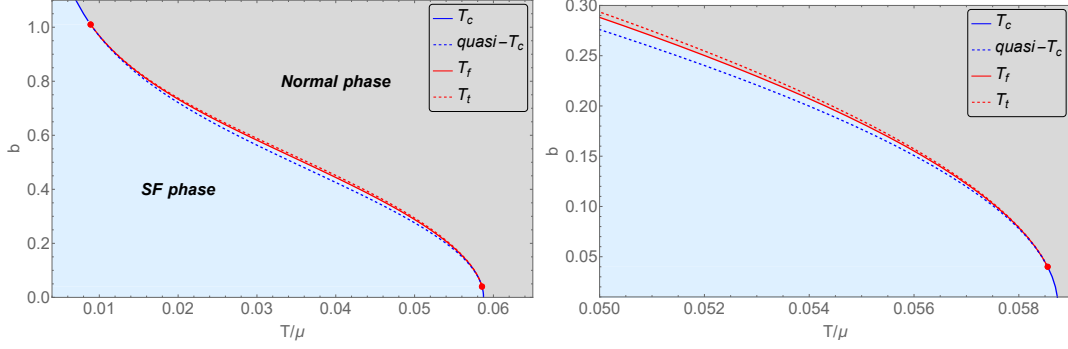


Figure 5: The phase diagram of temperature T/μ and back-reaction parameter b with $\lambda = -0.75$ and $\tau = 0.5$. The right panel is an enlarged view of a section of the left panel. The blue solid line represents the phase transition points of second-order phase transition. The blue dashed line represents the quasi-critical points of first-order phase transition at which the superfluid solution first appears. The red solid line represents the phase transition points of first-order phase transition. The red dashed line represents the turning points of first-order phase transition. The blue region corresponds to the superfluid phase.

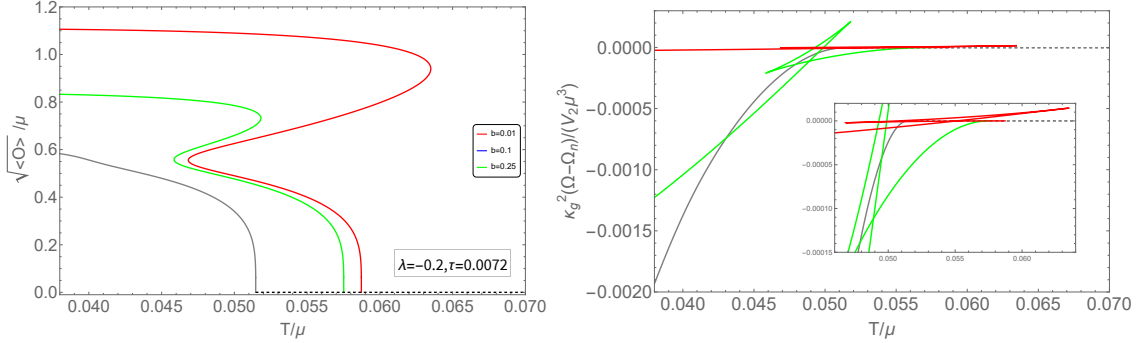


Figure 6: The dependence of the condensate curve on the back-reaction term b with parameters $\lambda = -0.2$ and $\tau = 0.0072$. The left panel depicts the condensate diagram, while the right panel represents the corresponding free energy. The red and green solid lines represent COW phase transition. The gray solid line represents second-order phase transition.

superfluid phases in the COW case ultimately terminates at a critical endpoint if we increase the value of τ [48]. Since the back-reaction strength bring in similar effects as the 6th power term coefficient τ , we set $\lambda = -0.2$ and $\tau = 0.0072$ and present the condensate curves with increasing values of the back-reaction strength b to see whether we are able to get the critical point.

We show the condensates as well as the grand potential curves with three values of the back-reaction strength b in Figure 6. We can see from this figure that with increasing value of the back-reaction strength, the swallow tail region in the first-order phase transition becomes narrow and finally disappears while the condensate curve become the typical second-order

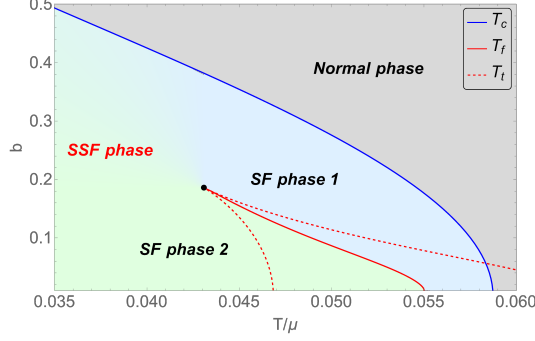


Figure 7: The phase diagram of temperature T/μ and back-reaction parameter b with $\lambda = -0.2$ and $\tau = 0.0072$. The blue solid line is the superfluid phase transition line. The red solid line represents the phase transition points of first-order phase transition between two different superfluid phases and the black point is the critical point of first-order phase transition. The SF represents Superfluid and the SSF represents Supercritical Superfluid. The red dashed lines are the spinodal region of first-order phase transition.

type.

Moreover, we build up the $b - T$ phase diagram from the phase transitions with various values of the back-reaction strength b and present the results in Figure 7. In this phase diagram, we see a critical point at the end of curve indicating the first-order phase transition points, beyond which is the supercritical region where the superfluid solutions with larger (SF phase 2) and smaller (SF phase 1) condensates are no longer distinguishable. This phase diagram is similar to the one with varying the value of τ instead of b , which again confirms our conjecture that the back-reaction strength bring in similar effective coupling as the 6th power term with coefficient τ .

4 The influence of λ and τ on phase transitions with finite back-reaction strength

With the two non-linear terms with coefficients λ and τ , various phase transitions are realized in the probe limit [47], which presents powerful control of λ and τ on the superfluid solutions. We have confirmed that this powerful control of λ and τ still work in a similar way when the back-reaction strength is finite, therefore we are able to tune the holographic superfluid phase transitions more accurately even with finite back-reaction strength.

Fixing the finite back-reaction strength $b = 0.2$, we illustrate the condensates as well as the grand potential curves with $\lambda = -0.2$ and different values of τ in Figure 8. From the two panels in Figure 8, we confirm that the effect of the increasing value of τ with finite back-reaction effect is the same as in the probe limit. With $\tau = 0$, the phase transition is likely to be zeroth-order as shown by the red curves. However, as we have explained in Section 3.2, the red solid line are expected to turn back at very large condensate to form the style of a

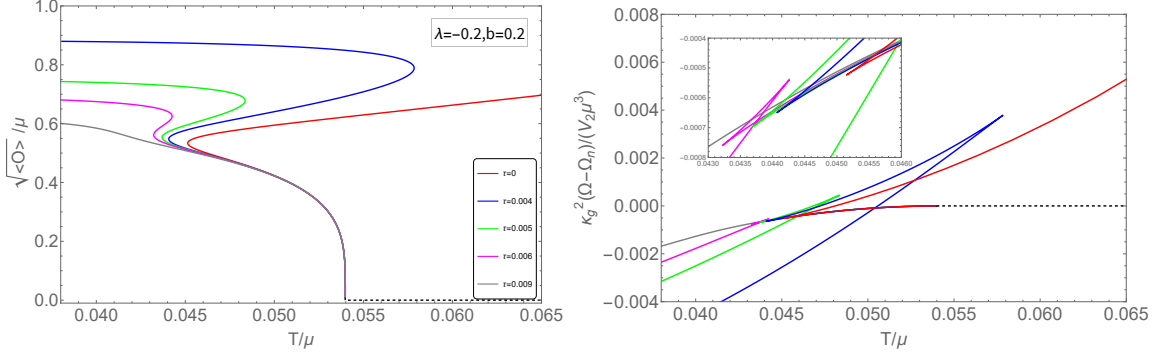


Figure 8: The dependence of the condensate curves on the self-interaction term τ with parameters $\lambda = -0.2$ and $b = 0.2$. The left panel depicts the condensate diagram, while the right panel represents the corresponding free energy. The red solid line represents first-order phase transition. The blue, green and magenta solid lines represent COW phase transition. The gray solid line represents second-order phase transition. The black dashed line is the normal solution.

first-order phase transition, due to the effective interaction introduced by the finite value of the back-reaction strength b . With the increasing value of τ , the superfluid phase transitions change from the first-order to the second-order, living a critical point at the end of the line of first-order phase transition points, which is the same as in the probe limit. The region of the supercritical superfluid is also available in this situation beyond the critical point.

At finite back-reaction strength, the 4th power term coefficient λ also show similar influence on the superfluid phase transitions as in the probe limit. Compared to the 6th power term coefficient τ , λ is more efficient on tuning the superfluid solutions near the critical point. We show the condensates as well as the grand potential curves with increasing values of λ in Figure 9, while fixing $\tau = 0$ and a finite back-reaction strength $b = 0.2$. We see clearly from the left panel that the red, blue, green, and magenta condensate curves grow leftward at the critical point, while the gray curve grows rightward. Notably, because a non-zero back-reaction strength introduces an effective coupling similar to a 6th power term with positive value of τ , all the condensate curves in Figure 9 should finally turn to grow leftward at sufficiently large condensate.

Similar to the case in probe limit, we see a special value λ_s , which divide the different growing direction of the condensate curve, and is important in switching between the first-order and second-order superfluid phase transitions. This special value should depend on the value of the back reaction strength. From the results in Section 3.3, the dependence of λ_s on b must be non-monotonic. We plot the dependence of λ_s on b in Figure 10. In this plot, the black curve show the dependence of the special value λ_s on the back reaction strength b , which dividing this parameter space into the left yellow part dominated by the first-order superfluid phase transition and the right blue part dominated by the second-order superfluid phase transition.

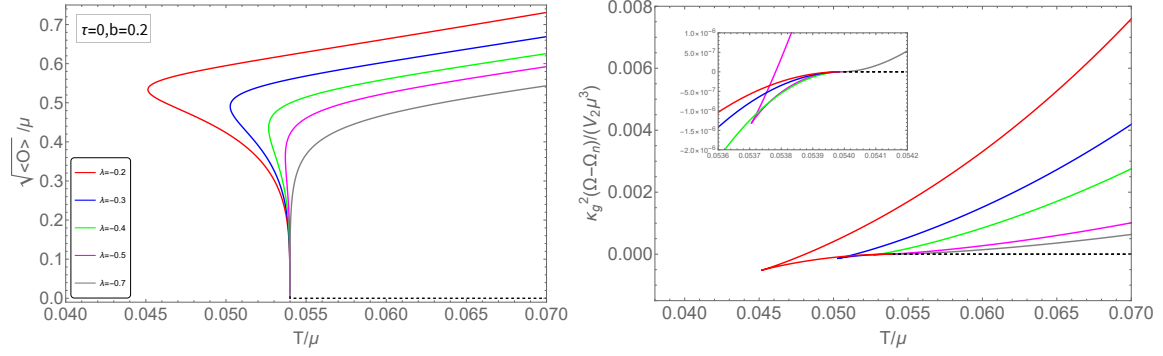


Figure 9: The dependence of the condensate curves on the self-interaction term λ with parameters $\tau = 0$ and $b = 0.2$. The left panel depicts the condensate diagram, while the right panel represents the corresponding free energy. The red, blue, green, magenta and gray solid lines represent first-order phase transition.

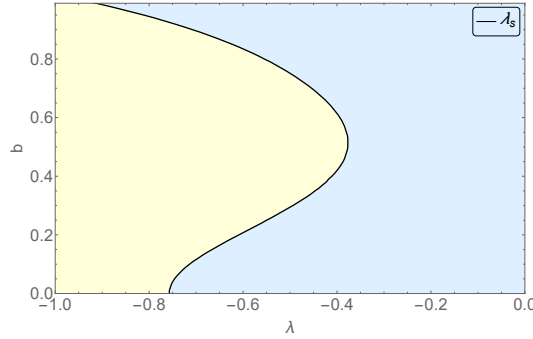


Figure 10: The phase diagram of critical λ_s and back-reaction parameter b . The blue region represents where the system has stable superfluid solutions, while the yellow region represents where the system does not have superfluid solutions.

5 Conclusions and discussions

In this work, we studied the phase transitions of the holographic s-wave superfluid model with the 4th and 6th power nonlinear terms beyond the probe limit. In such a setup, we are able to study the influence of the increasing back-reaction strength on the various phase transitions including the second order, the first order, the zeroth order as well as COW phase transitions. We are also able to confirm the universal control of the 4th and 6th power term coefficients λ and τ on the phase transitions beyond the probe limit. We further give the dependence of the special value λ_s , beyond which the condensate curve grows to an opposite direction at the critical point, on the back-reaction strength b .

In such a setup, we are also able to understand the effect of the finite back-reaction strength from an effective coupling point of view. It is already clear that increasing the back-reaction strength b will deform the back ground metric, therefore, the critical temperature

of the superfluid phase decreases. Following the condensates with increasing value of the back-reaction strength from the different phase transitions in the probe limit, we see that the back-reaction strength contains both the effective couplings similar to the 4th power and 6th power terms. This could be understood as that with finite back-reaction strength, the condensate of the scalar field deforms the metric tensor, while the deformation of the metric tensor again affects the scalar, which possibly brings in effective coupling similar to the 4th and 6th power terms. The effective coupling of the 6th power term from the back-reaction strength seems positive, while the effective coupling of the 4th power term might change the sign along with the increasing value of the back-reaction strength from the non-monotonic dependence of λ_s on b in Figure 10.

In Ref. [47], it is argued from the landscape analysis that as long as the 6th power coefficient τ gets a positive number, no matter how small it is, this term will dominate in the region with sufficiently large condensate, and stabilize the system by bounding the thermodynamic potential landscape from below. If the back-reaction strength also brings in an effective 6th power potential with positive coefficient, we can also confirm the stability of the system from the landscape point of view, and expect a stable superfluid phase with very large condensate at small value of the back-reaction strength b .

There are many interesting topics to be further investigated in future studies. It is interesting to confirm the effective couplings brought by the back-reaction strength by expanding the Lagrangian to linear level of the back-reaction strength b to get the effective action on the background metric. Then it is straight forward to see how the back-reaction affects the holographic superfluid phase transitions analytically. With the finite value of the back-reaction strength, it is possible to consider the entanglement entropy, the complexity as well as the black hole interior with various holographic superfluid phase transitions. From another perspective, the crossovers in the supercritical region are frequently mentioned in recent studies. This should be investigated in more detail in the future studies (see *e.g.* Refs. [50–55]). It is interesting to study the supercritical region in our $b - T$ phase diagram in Figure 7 to promote the studies on the holographic aspect of the gravity system.

Acknowledgements

This work was supported by National Natural Science Foundation of China (Grant Nos. 12473001, 11965013, 11975072), Yunnan High-level Talent Training Support Plan Young & Elite Talents Project (Grant No. YNWR-QNBJ-2018-181), the National SKA Program of China (Grant Nos. 2022SKA0110200, 2022SKA0110203), and the National 111 Project (Grant No. B16009).

References

- [1] J. M. Maldacena, The Large N limit of superconformal field theories and supergravity, [*Adv. Theor. Math. Phys.* **2** \(1998\) 231–252](#), [[hep-th/9711200](#)].
- [2] S. A. Hartnoll, C. P. Herzog and G. T. Horowitz, Building a Holographic Superconductor, [*Phys. Rev. Lett.* **101** \(2008\) 031601](#), [[0803.3295](#)].

- [3] S. A. Hartnoll, C. P. Herzog and G. T. Horowitz, Holographic Superconductors, [*JHEP* **12** \(2008\) 015](#), [[0810.1563](#)].
- [4] S. S. Gubser and S. S. Pufu, The Gravity dual of a p-wave superconductor, [*JHEP* **11** \(2008\) 033](#), [[0805.2960](#)].
- [5] R.-G. Cai, L. Li and L.-F. Li, A Holographic P-wave Superconductor Model, [*JHEP* **01** \(2014\) 032](#), [[1309.4877](#)].
- [6] J.-W. Chen, Y.-J. Kao, D. Maity, W.-Y. Wen and C.-P. Yeh, Towards A Holographic Model of D-Wave Superconductors, [*Phys. Rev. D* **81** \(2010\) 106008](#), [[1003.2991](#)].
- [7] K.-Y. Kim and M. Taylor, Holographic d-wave superconductors, [*JHEP* **08** \(2013\) 112](#), [[1304.6729](#)].
- [8] P. Basu, J. He, A. Mukherjee, M. Rozali and H.-H. Shieh, Competing Holographic Orders, [*JHEP* **10** \(2010\) 092](#), [[1007.3480](#)].
- [9] D. Musso, Competition/enhancement of two probe order parameters in the unbalanced holographic superconductor, [*JHEP* **06** \(2013\) 083](#), [[1302.7205](#)].
- [10] Z.-Y. Nie, R.-G. Cai, X. Gao and H. Zeng, Competition between the s-wave and p-wave superconductivity phases in a holographic model, [*JHEP* **11** \(2013\) 087](#), [[1309.2204](#)].
- [11] A. Donos, J. P. Gauntlett and C. Pantelidou, Competing p-wave orders, [*Class. Quant. Grav.* **31** \(2014\) 055007](#), [[1310.5741](#)].
- [12] Z.-H. Li, Y.-C. Fu and Z.-Y. Nie, Competing s-wave orders from Einstein–Gauss–Bonnet gravity, [*Phys. Lett. B* **776** \(2018\) 115–123](#), [[1706.07893](#)].
- [13] Z.-Y. Nie and H. Zeng, P-T phase diagram of a holographic s+p model from Gauss-Bonnet gravity, [*JHEP* **10** \(2015\) 047](#), [[1505.02289](#)].
- [14] Z.-Y. Nie, R.-G. Cai, X. Gao, L. Li and H. Zeng, Phase transitions in a holographic s + p model with back-reaction, [*Eur. Phys. J. C* **75** \(2015\) 559](#), [[1501.00004](#)].
- [15] I. Amado, D. Arean, A. Jimenez-Alba, L. Melgar and I. Salazar Landea, Holographic s+p Superconductors, [*Phys. Rev. D* **89** \(2014\) 026009](#), [[1309.5086](#)].
- [16] X. Qiao, L. OuYang, D. Wang, Q. Pan and J. Jing, Holographic superconductors in 4D Einstein-Gauss-Bonnet gravity, [*JHEP* **12** \(2020\) 192](#), [[2005.01007](#)].
- [17] J. Pan, X. Qiao, D. Wang, Q. Pan, Z.-Y. Nie and J. Jing, Holographic superconductors in 4D Einstein-Gauss-Bonnet gravity with backreactions, [*Phys. Lett. B* **823** \(2021\) 136755](#), [[2109.02207](#)].
- [18] X.-K. Zhang, Z.-Y. Nie, H. Zeng and Q. Pan, The holographic s+p model in 4D and 5D Einstein-Gauss-Bonnet gravity, [*Phys. Lett. B* **850** \(2024\) 138496](#), [[2306.13308](#)].

- [19] D. Ghorai and S. Gangopadhyay,
Analytical study of holographic superconductor with backreaction in 4d Gauss-Bonnet gravity,
[Phys. Lett. B](#) **822** (2021) 136699, [[2105.09423](#)].
- [20] R.-G. Cai and H.-Q. Zhang, Holographic Superconductors with Hořava-Lifshitz Black Holes,
[Phys. Rev. D](#) **81** (2010) 066003, [[0911.4867](#)].
- [21] H.-B. Zeng, C.-Y. Xia and A. del Campo,
Universal Breakdown of Kibble-Zurek Scaling in Fast Quenches across a Phase Transition,
[Phys. Rev. Lett.](#) **130** (2023) 060402, [[2204.13529](#)].
- [22] C.-Y. Xia, H.-B. Zeng, C.-M. Chen and A. del Campo,
Structural phase transition and its critical dynamics from holography, [Phys. Rev. D](#) **108** (2023)
026017, [[2302.11597](#)].
- [23] C.-Y. Xia, H.-B. Zeng, Y. Tian, C.-M. Chen and J. Zaanen,
Holographic Abrikosov lattice: Vortex matter from black hole, [Phys. Rev. D](#) **105** (2022)
L021901, [[2111.07718](#)].
- [24] X. Zhao, Z.-Y. Nie, Z.-Q. Zhao, H.-B. Zeng, Y. Tian and M. Baggioli,
Dynamical evolution of spinodal decomposition in holographic superfluids, [JHEP](#) **02** (2024)
184, [[2311.08277](#)].
- [25] J.-H. Su, C.-Y. Xia, W.-C. Yang and H.-B. Zeng,
Vortex-antivortex lattices in a holographic superconductor, [Phys. Rev. D](#) **109** (2024) 046019,
[[2311.05856](#)].
- [26] M. Baggioli and G. Frangi, Holographic supersolids, [JHEP](#) **06** (2022) 152, [[2202.03745](#)].
- [27] M. Baggioli and B. Goutéraux,
Colloquium: Hydrodynamics and holography of charge density wave phases, [Rev. Mod. Phys.](#)
95 (2023) 011001, [[2203.03298](#)].
- [28] M. Baggioli, Applied Holography: A Practical Mini-Course, other thesis, Madrid, IFT, 2019.
10.1007/978-3-030-35184-7.
- [29] M. Baggioli, L. Li and H.-T. Sun,
Shear Flows in Far-from-Equilibrium Strongly Coupled Fluids, [Phys. Rev. Lett.](#) **129** (2022)
011602, [[2112.14855](#)].
- [30] M. Baggioli, S. Grieninger, S. Grozdanov and Z. Lu,
Aspects of univalence in holographic axion models, [JHEP](#) **11** (2022) 032, [[2205.06076](#)].
- [31] D. Pan, T. Ji, M. Baggioli, L. Li and Y. Jin,
Nonlinear elasticity, yielding, and entropy in amorphous solids, [Sci. Adv.](#) **8** (2022) abm8028,
[[2108.13124](#)].
- [32] E. Witten, Introduction to Black Hole Thermodynamics, [2412.16795](#).
- [33] H.-Y. Chen, M. Fishbach and D. E. Holz,
A two per cent Hubble constant measurement from standard sirens within five years, [Nature](#)
562 (2018) 545–547, [[1712.06531](#)].
- [34] DES, LIGO SCIENTIFIC, VIRGO collaboration, M. Soares-Santos et al., First measurement of
the hubble constant from a dark standard siren using the dark energy survey galaxies and the

- ligo/virgo binary–black-hole merger gw170814, [Astrophys. J. Lett.](#) **876** (2019) L7, [[1901.01540](#)].
- [35] LIGO SCIENTIFIC, VIRGO, KAGRA collaboration, R. Abbott et al., Constraints on the Cosmic Expansion History from GWTC–3, [Astrophys. J.](#) **949** (2023) 76, [[2111.03604](#)].
- [36] J.-Y. Song, L.-F. Wang, Y. Li, Z.-W. Zhao, J.-F. Zhang, W. Zhao et al., Synergy between csst galaxy survey and gravitational-wave observation: Inferring the hubble constant from dark standard sirens, [Sci. China Phys. Mech. Astron.](#) **67** (2024) 230411, [[2212.00531](#)].
- [37] S.-J. Jin, Y.-Z. Zhang, J.-Y. Song, J.-F. Zhang and X. Zhang, Taiji-tianqin-lisa network: Precisely measuring the hubble constant using both bright and dark sirens, [Sci. China Phys. Mech. Astron.](#) **67** (2024) 220412, [[2305.19714](#)].
- [38] S.-J. Jin, R.-Q. Zhu, J.-Y. Song, T. Han, J.-F. Zhang and X. Zhang, Standard siren cosmology in the era of the 2.5-generation ground-based gravitational wave detectors: bright and dark sirens of ligo voyager and nemo, [JCAP](#) **08** (2024) 050, [[2309.11900](#)].
- [39] Y.-Y. Dong, J.-Y. Song, S.-J. Jin, J.-F. Zhang and X. Zhang, Enhancing dark siren cosmology through multi-band gravitational wave synergetic observations, [2404.18188](#).
- [40] S.-R. Xiao, Y. Shao, L.-F. Wang, J.-Y. Song, L. Feng, J.-F. Zhang et al., Nanohertz gravitational waves from a quasar-based supermassive black hole binary population model as dark sirens, [2408.00609](#).
- [41] J.-Y. Song, J.-Z. Qi, J.-F. Zhang and X. Zhang, Model-independent h_0 within flrw: Joint constraints from gwtc-3 standard sirens and strong lensing time delays, [2503.10346](#).
- [42] R.-G. Cai, L. Li, L.-F. Li and Y.-Q. Wang, Competition and Coexistence of Order Parameters in Holographic Multi-Band Superconductors, [JHEP](#) **09** (2013) 074, [[1307.2768](#)].
- [43] Y.-Q. Wang and S. Liu, Holographic s-wave and p-wave Josephson junction with backreaction, [JHEP](#) **11** (2016) 127, [[1608.06364](#)].
- [44] Y.-Q. Wang, H.-B. Li, Y.-X. Liu and Y. Zhong, Excited states of holographic superconductors with backreaction, [Eur. Phys. J. C](#) **81** (2021) 628, [[1911.04475](#)].
- [45] M. Ammon, J. Erdmenger, V. Grass, P. Kerner and A. O’Bannon, On Holographic p-wave Superfluids with Back-reaction, [Phys. Lett. B](#) **686** (2010) 192–198, [[0912.3515](#)].
- [46] R.-G. Cai, L. Li, L.-F. Li and R.-Q. Yang, Towards Complete Phase Diagrams of a Holographic P-wave Superconductor Model, [JHEP](#) **04** (2014) 016, [[1401.3974](#)].
- [47] Z.-Q. Zhao, X.-K. Zhang and Z.-Y. Nie, Dynamical stability from quasi normal modes in 2nd, 1st and 0th order holographic superfluid phase transitions, [JHEP](#) **02** (2023) 023, [[2211.14762](#)].
- [48] Z.-Q. Zhao, Z.-Y. Nie, J.-F. Zhang, X. Zhang and M. Baggioli, Dynamical and thermodynamic crossovers in the supercritical region of a holographic superfluid model, [Eur. Phys. J. C](#) **85** (2025) 464, [[2406.05345](#)].

- [49] R.-G. Cai, Constant curvature black hole and dual field theory, [Phys. Lett. B **544** \(2002\) 176–182](#), [[hep-th/0206223](#)].
- [50] J. Das Bairagya, K. Pal, K. Pal and T. Sarkar, The geometry of RN-AdS fluids, [Phys. Lett. B **805** \(2020\) 135416](#), [[1912.01183](#)].
- [51] A. Sahay and R. Jha, Geometry of criticality, supercriticality and Hawking-Page transitions in Gauss-Bonnet-AdS black holes, [Phys. Rev. D **96** \(2017\) 126017](#), [[1707.03629](#)].
- [52] S.-W. Wei, Y.-X. Liu and R. B. Mann, Ruppeiner Geometry, Phase Transitions, and the Microstructure of Charged AdS Black Holes, [Phys. Rev. D **100** \(2019\) 124033](#), [[1909.03887](#)].
- [53] S.-W. Wei and Y.-X. Liu, Thermodynamic nature of black holes in coexistence region, [Sci. China Phys. Mech. Astron. **67** \(2024\) 250412](#), [[2308.11886](#)].
- [54] Z.-Q. Zhao, Z.-Y. Nie, J.-F. Zhang and X. Zhang, The universal crossover from thermodynamics and dynamics of supercritical RN-AdS black hole, [2504.04995](#).
- [55] Z.-M. Xu and R. B. Mann, Thermodynamic supercriticality and complex phase diagram for the AdS black hole, [2504.05708](#).